Exploiting the Differential Wavelet Domain of Resting-State EEG Using a Deep-CNN for Screening Parkinson's Disease

Mohamed Shaban*, Stephen Cahoon, Fiza Khan, and Mahalia Polk
Electrical and Computer Engineering Department
University of South Alabama
Mobile, Alabama, United States
*Corresponding author: mshaban@southalabama.edu

2021 IEEE Symposium Series on Computational Intelligence (SSCI) | 978-1-7281-9048-8/21/$31.00 ©2021 IEEE | DOI: 10.1109/SSCI50451.2021.9660178

Abstract— **In this paper, a deep Convolutional Neural Network (CNN) of 20 layers was deployed to exploit the features extracted from the Laplacian of the Wavelet transform of a resting-state EEG time-series dataset in order to distinguish persons with Parkinson's disease (PD) from healthy controls (HC). It was shown that PD presents significant discriminative changes in the differential Wavelet domain as compared to HC especially at intermediate and lower scales. Due to the observed discrepancies, the deep CNN method was able to identify subjects with PD at a 4-fold as well as 10-fold cross-validation accuracy, sensitivity, and specificity of up to 99.9% surpassing most of the-state-of-the-art deep learning-based architectures.**

Keywords— Parkinson's Disease, Wavelet Transform, Laplacian, Convolutional Neural Networks

I. Introduction

Parkinson's disease (PD) is a serious neurodegenerative disorder with symptoms that may include hand tremors, bradykinesia, limb rigidity, gait and balance problems, speech and sleep behavior disorders [1]. Early diagnosis and screening is crucial to potentially slow down the progression of the disease via efficient administered therapeutic treatments. Until now, there are no established or unique biomarkers of PD that can be adopted by clinicians for disease diagnosis and staging.

It has been recently shown that Electroencephalography (EEG) of subjects with PD shows decreased beta and gamma powers [2-4], and related phase-amplitude coupling changes with respect to healthy controls (HC) [5] [6].

In addition, machine and deep learning (MDL) techniques were introduced as an alternative to standard spectral analysis methods to classify and diagnose PD with performance that widely varied from 83% to 100% [7-15].

In this study, we investigate the use of a deep learning framework that exploits the differential Wavelet domain of a resting-state EEG time-series captured for subjects with PD and HC achieving elevated accuracy, sensitivity, and specificity as compared with the-state-of-the-art approaches presented [7-13] and a comparable performance with respect to the most recent work presented in [14] [15].

II. PD Detection Using Machine and Deep Learning Applied on EEG

MDL techniques were recently adopted to classify PD from the EEG time-series data [7-15]. Vanegas et al. proposed extra trees (which combines predictions of several decision trees), linear regression, and decision tree to predict biomarkers of PD with a best-case area under the curve (AUC) of 99.4% [7]. Oh et al. developed a Convolutional Neural Network (CNN) structure to identify new PD subjects with an accuracy of 88.3% [8]. Wagh et al. introduced a graph CNN to classify subjects into "diseased" including patients with PD and "healthy" at a 10-fold cross validation accuracy of 85% [9]. Koch et al. used a random forest classifier to detect PD with an AUC of 91% [10]. Shi et al. and Lee et al. proposed hybrid CNN-Recurrent Neural Network (RNN) models to detect PD with an accuracy of 82.9% and 96.9% respectively [11] [12]. In [13], our prior work adopted an ANN-based framework applied on three spatial channels of EEG including Oz, P8, and FC2 to distinguish PD from HC with an accuracy of 98%, sensitivity of 97%, and specificity of 100%. Khare et al. have recently introduced the use of pseudo-Wigner Ville distribution along with a 2D-CNN on two datasets with a validation accuracy of 100% and 99.9% respectively [14]. Using Gabor transform and a deep CNN, Loh et al. were able to classify subjects into HC and PD with and without medications at an accuracy of 99.5% [15].

III. Proposed Wavelet-Based CNN Method

A. Dataset Description

The EEG dataset was created in the Aron lab at the University of California at San Diego and analyzed in the Swann lab at the University of Oregon. The dataset is available on OpenNeuro with the latest version of 1.0.4 published in January 2021 [16].

The dataset includes EEG samples for fifteen right-handed PD patients (eight females, mean age 62.6 ± 8.3 years old), and sixteen matched HC (nine females, 63.5 ± 9.6 years). All PD patients have either mild or moderate PD. The EEG data were recorded at a sampling rate of 512 S/s within 1.9 to 2 minutes using thirty-two standard electrodes. The locations of the 32-channel EEG electrodes are shown in fig. 1.

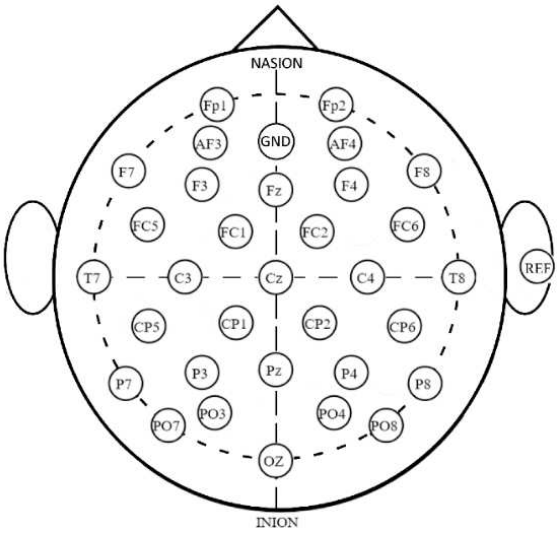

Fig. 1. Locations of 32-electrodes of EEG

B. Proposed Method

The EEG signal *x(t)* recorded at the i^{th} electrode ($x_i(t)$) was transformed into the Wavelet domain using the Continuous Wavelet Transform (CWT) defined as follows:

$$X_i(s) = \frac{1}{\sqrt{s}} \int_0^{\infty} x_i(t)\, \psi\left(\frac{t}{s}\right) dt \qquad (1)$$

where ψ is the Morlet analysis Wavelet, and *s* is the scale of the Wavelet. The scale is inversely proportional to the Fourier frequencies which roughly extend from 0 to 190 Hz within the recorded EEG data.

Further, the absolute values of $X_i(s)$ were calculated and further scaled-up by a factor of α (i.e., 500) to emphasize on the slight changes and deviations in the Wavelet domain. The generated values of $\alpha|X_i(s)|$ have an approximate dimension of 138×96,768 for HC and 138×97,792 for PD.

A Laplacian filter was applied on $|\alpha X_i(s)|$ to detect changes in the Wavelet domain across various scales and time intervals. The selected Laplacian kernel is defined as follows:

$$L = \begin{bmatrix} 0 & -1 & 0 \\ -1 & 4 & -1 \\ 0 & -1 & 0 \end{bmatrix} \qquad (2)$$

where L was moved over $|\alpha X_i(s)|$ matrix (stride of one) and the sums of products at each position was determined. The outputs of the Laplacian filter were segmented in time into 128×128 samples where the components corresponding to the highest 10 scales or the lowest 10 frequencies were discarded. The previously mentioned filtered and segmented outputs were then converted into gray-scale images with 128×128×1 dimension. Examples of images corresponding to HC and PD for the EEG signal recorded at Fp1 electrode are shown in Fig. 2.

Gray-scale images corresponding to HC are brighter with respect to PD images especially at low and intermediate scales (i.e., high and intermediate frequencies). This may imply that subjects with PD exhibit slow-changes in the Wavelet domain at the aforementioned scales. This is a quite novel interesting observation that may need to be further investigated in a clinical research study.

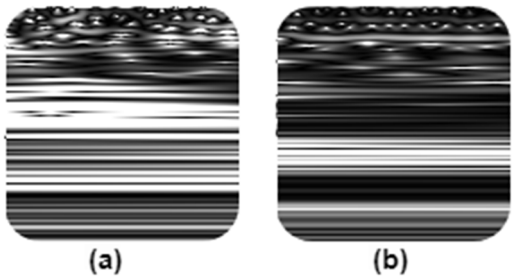

Fig. 2. Scalogram representing the Differential EEG Wavelets recorded at Fp1 for (a) HC and (b) PD

Based on this significant discriminative feature observed in the differential Wavelet domain, we introduced the use of a successful CNN proposed by Shaban et al. in [17] to detect oil spills from satellite aperture radar images on the differential Wavelets of HC and PD. The structure of the proposed CNN is represented in Table 1. The proposed network consists of 20 layers of convolutional, rectified linear units (ReLU), and maximum pooling (MaxPooling) stages. The CNN was originally developed using the grid search algorithm [18] where the hyper-parameters of the network were varied and the validation accuracy was monitored. Fig. 3 shows the block diagram of the proposed approach.

C. Evaluation Metrics

Both four-fold and ten-fold cross-validation techniques were used to assess the ability of the proposed CNN to distinguish subjects with PD from HC. The Quadratic weighted Kappa score (*K*) was used as well such that:

$$K = 1 - \frac{\sum_{m=0}^{2}\sum_{n=0}^{2} w(m,n)c(m,n)}{\sum_{m=0}^{2}\sum_{n=0}^{2} w(m,n)p(m,n)} \qquad (3)$$

where *w(m,n), c(m,n),* and *p(m,n)* are the elements of the weight matrix *W*, the normalized confusion matrix *C*, and the outer product of predicted/actual histograms matrix *P* respectively.

TABLE 1. CNN STRUCTURE

Layer	Layer Dimension	No. of Layers	No. of Feature Maps
Input Image	128×128	1	-
Convolutional with ReLU	11×11	4	32
Maximum Pooling	2x2	1	32
Convolutional with ReLU	9×9	4	64
Maximum Pooling	2x2	1	64
Convolutional with ReLU	7×7	4	128
Maximum Pooling	2×2	1	128
Fully Connected with ReLU	128, 64, 32, 16	4	-
Fully Connected with SoftMax	2	1	-

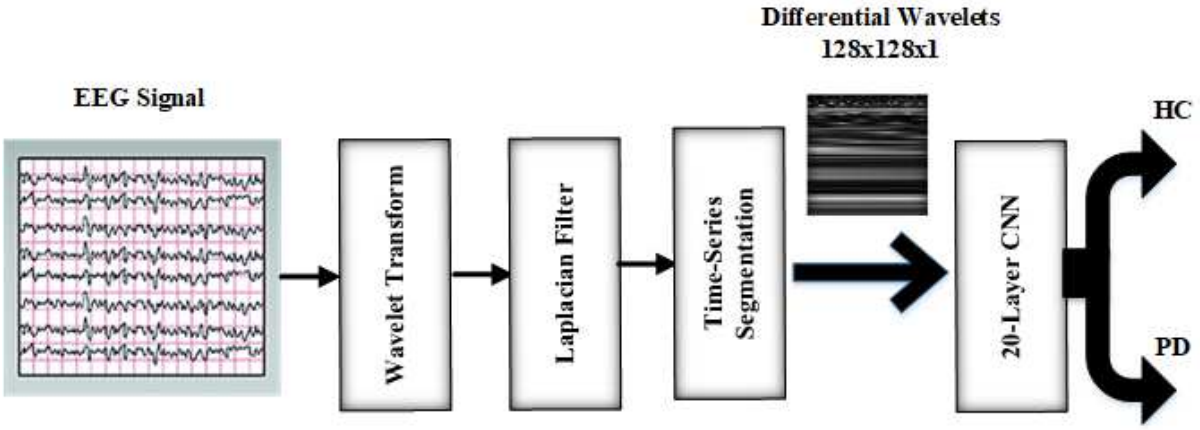

Fig. 3. Proposed differential Wavelet-based CNN approach

IV. EXPERIMENTAL RESULTS

Differential Morlet Wavelet transform was applied on the 31 tables corresponding to the EEG time-series signals for the 16 HC and 15 PD (OFF medication) generating 24,264 gray-scale images of a dimension 128×128×1 for each of the 32 spatial channels. A total of 12,260 images were labelled as HC while 12,004 were related to PD.

Next, the proposed CNN structure was then trained on the images of five different channels (i.e. Fp1, FC1, CP5, P8 and Fz) which were selected on a random basis spanning different spatial locations on the scalp (see Fig. 1) for 40 epochs. A batch size, learning rate, decay rate, and momentum of 50, 5×10^{-5}, 0.1, and 0.9 were selected as the hyperparameters of the model. Both 4-fold and 10-fold cross-validation methods were used to evaluate the performance of the model where the training and validation images did not overlap and were selected on a random basis.

Table 2 and Table 3 present the 4-fold and 10-fold cross-validation accuracy, sensitivity, specificity, weighted Kappa score, and AUC respectively for the five different channels.

TABLE 2. 4-FOLD CROSS VALIDATION RESULTS

Channel	(Fp1)	(FC1)	(CP5)	(P8)	(Fz)
Accuracy	99.8%	99.9%	99.9%	99.9%	99.9%
Sensitivity	99.9%	99.9%	100%	99.9%	99.9%
Specificity	99.8%	99.9%	99.9%	99.9%	99.9%
Kappa Score	0.99	0.99	0.99	0.99	0.99
AUC	0.99	0.99	0.99	0.99	0.99

TABLE 3. 10-FOLD CROSS VALIDATION RESULTS

Channel	(Fp1)	(FC1)	(CP5)	(P8)	(Fz)
Accuracy	99.9%	99.9%	99.9%	99.9%	99.9%
Sensitivity	99.9%	99.9%	100%	99.9%	99.9%
Specificity	99.9%	99.9%	99.9%	99.9%	99.9%
Kappa Score	0.99	0.99	0.99	0.99	0.99
AUC	0.98	0.98	0.98	0.99	0.99

Based on the tables, the accuracy, sensitivity and specificity maintain a significantly high value of a minimum of 99.8% and maximum of 99.9% across the five selected channels when both 4-fold and 10-fold cross validation mechanisms were used. The weighted Kappa score was almost 0.99 showing a very limited bias of the proposed model and indicating that the agreements between the predicted and ground truth

labels did not take place by chance. Table 4 shows the confusion matrix for three randomly selected channels (i.e. Fp1, CP5 and Fz) with extremely high true positive and true negative rates.

TABLE 4. CONFUSION MATRIX FOR THE PROPOSED APPROACH (4-FOLD CROSS VALIDATION)

(Fp1)		
	HC	**PD**
HC	3066	3
PD	2	2995
(CP5)		
	HC	**PD**
HC	3114	1
PD	0	2951
(Fz)		
	HC	**PD**
HC	3044	2
PD	0	3020

When compared with the related state-of-the-art work presented in [12] [13] that deploy hybrid CNN-RNN and ANN respectively for PD classification and detection, the proposed approach achieved a significantly higher testing accuracy of up to 99.9% (see Table 5) and almost similar performance as the high performing methods proposed in [14] [15]. Based on the reported results, we claim that the proposed framework will provide an efficient, objective and precise computer-aided diagnostic tool that can be adopted by physicians to support the clinical diagnosis of the disease.

TABLE 5. COMPARISON OF THE PROPOSED APPROACH AND THE-STATE-OF-THE-ART ARCHITECTURES USED FOR PD DETECTION

Method	**Proposed**	**[12]**	**[13]**	**[14]**	**[15]**
Accuracy	99.9%	93%	98%	100%	99.5%

V. CONCLUSIONS

In this paper, we have proposed a CNN-based framework that automatically extracts PD features and classifies subjects into HC and PD based on the second-order derivative of the Wavelet transform of resting-state EEG.

First, the proposed method deployed a Morlet Wavelet transform at 128 different scales on the EEG data, and further applied a Laplacian filter to identify the changes in the Wavelet regions. The generated differential Wavelets were then split into patches of 128 time-series signals and transformed into 128×128 gray-scale images. A 20-layer CNN was finally applied for classifying subjects into HC and PD.

Significant discrepancies among the HC and PD cohorts were observed especially at low and intermediate Wavelet scales. As a result, the 20-layer CNN structure was able to efficiently distinguish between subjects with PD and HC at a very high 4-fold as well as 10-fold cross-validation accuracy, sensitivity and specificity of up to 99.9% outperforming the recent state-of-the-art deep learning architectures [12] [13] and offering a comparable performance as compared with the methods recently proposed in [14] [15]. This approach may serve as a computer-aided diagnostic tool offering an objective and reliable prediction of the presence of the disease based on resting-state EEG. This work also highlighted the significance of the higher-order derivatives of the Wavelet domain of resting-state EEG that may potentially present potential biomarkers of PD.

Based on the promising results achieved by the proposed approach, we plan to investigate the use of AI to exploit higher order derivatives of the Wavelet domain of EEG to classify the disease based on the presence of mild cognitive impairment and progression to advanced dementia. Further, the use of EEG datasets recorded for PD subjects who were later diagnosed with PD may offer a potential application of deep learning for the pre-clinical diagnosis of the disease.

It is also worth to investigate the application of AI on EEG with the motion artifacts being removed using the independent component analysis (ICA) technique as this may provide more emphasis on the actual discrepancies between HC and subjects with PD. In addition, since the CWT is a highly redundant transform where there is usually an overlap among Wavelets at different scales, Discrete Wavelet Transform (DWT) can replace the CWT to provide more efficient and sparse representation for the EEG signals.

ACKNOWLEDGMENT

Partial support of this research was provided by the Woodrow W. Everett, Jr. SCEEE Development Fund in cooperation with the Southeastern Association of Electrical Engineering Department Heads.

REFERENCES

[1] W. Dauer, and S. Przedborski, "Parkinson's disease: mechanisms, and models", *Neuron,* Vol. 39, no. 6, pp. 889-909, 2003.

[2] L. Pezard, R. Jech, and E. Ruzicka, "Investigation of non-linear properties of multichannel EEG in the early stages of Parkinson's disease", *Clinical Neurophysiology*, Vol. 165, no. 1, pp. 38-45, 2001.

[3] J. Bosboom, D Stoffers, C. Stam, B. Dijk, J. Verbunt, H. Berendse, and E. Wolters, "Resting state oscillatory brain dynamics in Parkinson's disease: an MEG study", *Clinical Neurophysiology*, Vol. 117, no. 11, pp. 2521-2531, 2006.

[4] R Soikkeli, J. Partanen, H. Soininen, A. Pääkkönen, and P. Riekkinen, "Slowing of EEG in Parkinson's disease", *Electroencephalography, and Clinical Neurophysiology*, Vol. 79, no. 3, pp. 159-165, 1991.

[5] C. Hemptinne, E. Ryapolova-Webb, E. Air, P. Garcia, K. Miller, J. Ojemann, J. Ostrem, N. Galifianakis, and P. Starr, "Exaggerated phase-amplitude coupling in the primary motor cortex in Parkinson disease", *Proceedings of National Academy of Sciences of the United States of America*, Vol. 110, pp. 4780–4785, 2013.

[6] N. Swann, C. Hemptinne, A. Aron, J. Ostrem, R. Knight, and P. Starr, "Elevated synchrony in Parkinson disease detected with electroencephalography", *Annals of Neurology,* Vol. 78, pp.742–750, 2015.

[7] M. Vanegas, M. Ghilardi, S. Kelly, and A. Blangero, "Machine Learning for EEG-Based Biomarkers in Parkinson's Disease", *IEEE International Conference on Bioinformatics and Biomedicine*, Madrid, Spain, 2018.

[8] S. Oh, Y. Hagiwara, U. Raghavendra, et al., "A deep learning approach for Parkinson's disease diagnosis from EEG signals", *Neural Computing and Applications*, Vol. 32, pp. 10927-10933, 2020.

[9] N. Wagh, and Y. Varatharajah, "EEG-GCNN: Augmenting Electroencephalogram-Based Neurological Disease Diagnosis Using a Domain-Guided Graph Convolutional Neural Network", *Machine Learning Research,* Vol. 136, pp. 367-378, 2020.

[10] M. Koch, V. Geraedts, et al., "Automated Machine Learning for EEG-Based Classification of Parkinson's Disease Patients", *IEEE International Conference on Big Data*, Los Angeles, USA, 2019.

[11] X. Shi, T. Wang, et al., "Hybrid Convolutional Recurrent Neural Networks Outperform CNN and RNN in Task-State EEG Detection for Parkinson's Disease", *Asia-Pacific Signal and Information Processing Association Annual Summit and Conference*, Lanzhou, China, 2019.

[12] S. Lee, R. Hussein, and M. McKeown, "A Deep Convolutional-Recurrent Neural Network Architecture for Parkinson's Disease EEG Classification", *IEEE Global Conference on Signal and Information Processing*, Ottawa, Canada, 2019.

[13] M. Shaban, **"**Automated Screening of Parkinson's Disease Using Deep Learning Based Electroencephalography", *International IEEE EMBS Conference on Neural Engineering*, Virtual, 2021.

[14] S. Khare, V. Bajaj, and U. Acharya, "PDCNNet:An Automatic Framwork for the Detection of Parkinson's Disease Using EEG Signals", *IEEE Sensors Journal*, Vol. 21, no. 15, pp. 17017-17024, 2021.

[15] H. Loh, C. Ooi, E. Palmer, P. Barua, S. Dogan, et al., "GaborPDNet: Gabor Transformation and Deep Neural Network for Parkinson's Disease Detection Using EEG Signals", *Electronics*, MDPI, Vol. 10, no. 14, Page 1740, 2021.

[16] A. Rockhill, N. Jackson, J. George, A. Aron, and N. Swann, "UC San Diego Resting State EEG Data from Patients with Parkinson's Disease", 2020. Available: https://openneuro.org/datasets/ds002778/versions/1.0.4

[17] M. Shaban, R. Salim, H. Abu Khalifeh, et al., "A Deep-Learning Framework for the Detection of Oil Spills from SAR Data", *Sensors,* MDPI, Vol. 21, no. 7, 2021.

[18] J. Dufour, and J. Neves, "Finite-Sample Inference and nonstandard asymptotics with Monte Carlo Tests and R" in *Handbook of Statistics*, Elsevier*,* Vol. 41, pp. 3-31, 2019.